ACS APPLIED MATERIALS & INTERFACES

Research Article

www.acsami.org

EBSD and EDX Analyses of a Multiphase Glass-Ceramic Obtained by Crystallizing an Yttrium Aluminosilicate Glass

Ashkan Keshavarzi, Wolfgang Wisniewski,* and Christian Rüssel

Otto-Schott-Institut, Jena University, Fraunhoferstrasse 6, 07743 Jena, Germany

ABSTRACT: A glass with the mol % composition 23.82 Y_2O_3·39.82 Al_2O_3·28.50 SiO_2·2.91AlF_3·4.95 ZrO_2 doped with 2 mol % CeF_3 is crystallized at 1250 °C for 20 h. The crystallized samples are studied using X-ray diffraction (XRD), the SEM-based methods EBSD and EDX, as well as fluorescence microscopy. Six crystalline phases are detected in the residual glass including alumina, YAG, Y-stabilized zirconia (YSZ), and three different yttrium silicates of the composition $Y_2Si_2O_7$. Chemistry-assisted indexing (ChI) is successfully applied to separate YAG and YSZ in EBSD-scans. YAG displays polygon as well as dendritic growth. Some crystals show both mechanisms at opposite ends, indicating that the growth mechanism is influenced by the chemistry of the surrounding glass matrix.

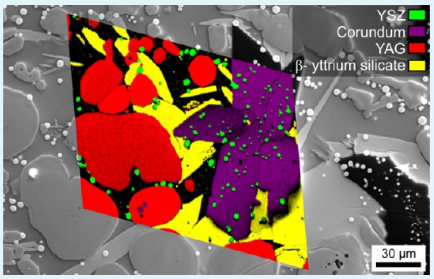

KEYWORDS: *YAG, glass crystallization, EBSD, phase identification*

INTRODUCTION

In the past few years, the crystallization of yttrium aluminum garnet (YAG) from glasses has been studied because of the potential of these materials in lighting and optic technologies.[1−6] Nowadays, most commercial white light emitting diodes (LEDs) use a GaInN blue emitter with an emission peak at 460 nm in combination with a YAG:Ce^{3+} yellow phosphor.[4] Currently, YAG powders embedded in polymers such as polysiloxanes are generally used despite their poor thermal conductivity which prevents an effective removal of the heat generated in the phosphor. This limits the maximum light intensity of LEDs especially for high power applications. These problems are less significant when using crystallized YAG in an inorganic glass matrix which is furthermore very stable against corrosion. Unfortunately, yttrium alumo silicates do not possess a high tendency towards the crystallization of YAG. High temperatures are usually necessary to crystallize these glasses, which then in turn may lead to the crystallization of other phases such as an Al-rich phase and various yttrium silicates.[6] Unfortunately, the crystallization of YAG from glasses is difficult to achieve and hence scarcely described in the literature. Nevertheless, there are some reports on the spontaneous crystallization of YAG while cooling a melt[7] and the controlled crystallization of YAG from glasses.[2,3,6] The nucleation in the melt and the subsequent crystal growth kinetics are notably affected by the diffusion of components from the glassy matrix to the interface crystal/glass and vice versa. Chemical variations may significantly change the growth mechanisms of YAG in glass as well as nucleation rates.[3] The growth of YAG in glasses has been described to lead to polygon structures[3] as well as to dendrites.[2,6]

The transparency of the glass-ceramics is usually discussed in terms of light scattering by crystals dispersed in a glass matrix. However, good transparency requires low optical scattering and low atomic absorption. The attenuation of light due to scattering depends upon the difference in the refractive indices of the two phases and the size and distribution of crystals in the glass. While the size of the crystals must usually be smaller than the wavelength of light if scattering and diffraction is to be avoided, recently prepared glass-ceramics containing large crystals also show a high transparency due to adapted diffractive indices.[8] Some traditional transparent glass-ceramics contain fairly large volume concentrations of crystals (up to 85%) but do not scatter light due to the small crystal size.[9−11] A possible strategy to avoid light scattering is to prepare a material with crystallite sizes notably smaller than half the wavelength of visible light (usually <50 nm) or only produce a thin surface layer of YAG.[4,6,12] For lighting, the light conversion from blue LEDs to white light does not necessarily require a material without any light scattering.

In this work, we present the crystallization of multiple phases from a glass including Ce^{3+}-doped YAG of both dendritic and polygon morphology. The sensitivity of phase formation and crystal growth with respect to the glass chemistry is illustrated by the contrast between homogeneous glass and a stria of different composition.

EXPERIMENTAL APPROACH

A glass of the mol % composition 23.82Y_2O_3·39.82Al_2O_3·28.50SiO_2·2.91AlF_3·4.95ZrO_2 doped with 2 mol % CeF_3 was prepared from reagent grade raw materials. A mixed batch of 100 g of raw oxides was melted for 3 h in a platinum−rhodium crucible using an electric furnace heated to 1590 °C. The melt was stirred manually to homogenize it and finally cast on a copper block, quenched with a copper stamp, and transferred to a furnace preheated to 850 °C, which was subsequently switched off, cooling the glass with a rate of about 5 K/min.

Received: May 22, 2013
Accepted: July 12, 2013
Published: July 12, 2013

   dx.doi.org/10.1021/am401953j | *ACS Appl. Mater. Interfaces* 2013, 5, 8531−8536

Differential thermal analyses (Shimadzu DTA50) were performed using Al_2O_3 powder as a reference standard and a heating rate of 5 K/min from room temperature to 1300 °C. To study the crystallization behavior, we cut the glass into pieces of about 1 × 1 × 1 cm^3 and transferred them to a furnace preheated to 800 °C, heated them to 1250 °C using a rate of 10 K/min where they were kept for 20 h. Finally, the furnace was switched off and the samples cooled with a rate of approximately 5 K/min.

The glass and annealed samples were characterized by X-ray diffraction in a θ-2-θ-setup (Siemens D5000) using $Cu_{K\alpha}$ radiation. The glass-ceramics were further characterized using a Jeol JSM-7001F scanning electron microscope (SEM) equipped with an EDAX Trident analyzing system containing a TSL Digiview 3 EBSD-camera. Samples were mounted using Ag paste and coated with a thin layer of carbon at about 1 × 10^{-3} Pa to achieve a conductive surface. EBSD scans were collected and evaluated using the programs TSL OIM Data Collection 5.31 and TSL OIM Analysis 5.31. EBSD data acquisition was performed using a accelerating voltage of 20 kV.

RESULTS AND DISCUSSION

The prepared glass was yellowish and optically transparent. The glass transition temperature T_g determined by dilatometry was 860 °C. Figure 1 presents XRD-patterns obtained from the solid glass and from a sample annealed at 1250 °C (390 K above T_g) for 20 h and powdered for XRD analysis. While the casted glass is X-ray amorphous; the annealed sample shows distinct XRD-lines which are all attributable to YAG (JCPDS file 82−0575) and yttrium-stabilized zirconia (YSZ, JCPDS file 037−1307). Other phases are not indicated by XRD.

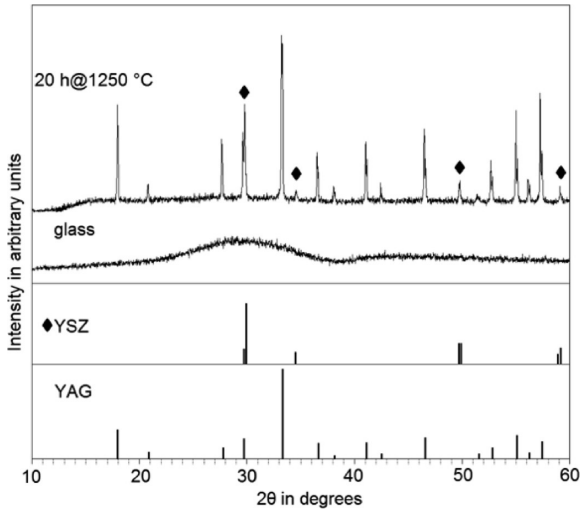

Figure 1. XRD pattern of the glassy sample and the samples crystallized at 1250 °C for 20 h.

A photograph of the polished surface of a sample annealed for 20 h is presented in Figure 2a. A white stria is discernible near the top of the otherwise yellow sample. The framed area is presented in the SEM micrograph of Figure 2b, which already reveals the presence of more phases than indicated by XRD analysis. The EBSD patterns of six crystalline phases are presented below, most of which may also be discerned by their SEM contrast. Pattern 1 was obtained from the darkest phase in the SEM-micrograph and may be well-indexed as α-Al_2O_3 (corundum). The dark gray phase forming the polygon structures outside the stria and the finer structures inside the stria are both YAG (pattern 2, ICSD-file 74607). The slightly brighter structures in the SEM micrograph provide the EBSD

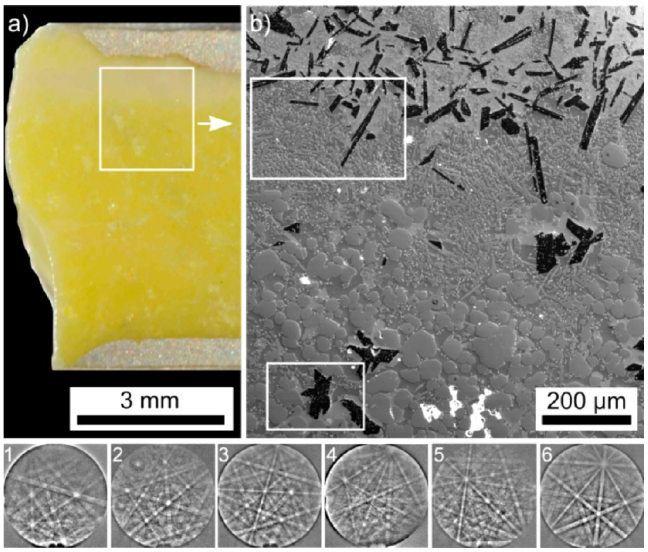

Figure 2. (a) Image of the polished surface of a sample crystallized at 1250 °C for 20 h. (b) SEM micrograph of the area framed in a. The areas framed in b are presented in the Figures 3 and 5 in greater detail. The EBSD patterns 1−6 were obtained from different crystal phases in the sample.

patterns 3−5, which may all be indexed as yttrium silicates (YS) of the composition $Y_2Si_2O_7$ and are not easily separated by their SEM contrast. Pattern 3 indicates monoclinic ε-$Y_2Si_2O_7$ (ε-YS, ICSD-file 28004), whereas pattern 4 indicates orthorhombic δ-$Y_2Si_2O_7$ (δ-YS, ICSD-file 33721). Both of these phases are detected only inside the stria, whereas the third YS indicated by pattern 5 is monoclinic β-$Y_2Si_2O_7$ (β-YS, ICSD-file 281312) and only found outside the stria.

The smallest crystals are very bright but difficult to discern at this magnification and may also be indexed as YAG although they clearly have a different mean atomic number. EDX-analyses were performed and confirmed the chemical compositions of the previously described phases. The bright phase showed a composition of 27.7Zr·11.6Y·59.2O·1.0Ce·0.5 Al (at %), meaning this is the YSZ indicated by XRD where some of the Y has been substituted by Ce and Al was basically expelled from the crystal during its growth. Although YAG and YSZ share the same cubic space group, the a-axis of YAG (ICSD-file 74607, a = 12.024 Å) is more than twice as large as that of YSZ (ICSD-file 164864, a = 5.165 Å). It is hence possible to distinguish these phases in the EBSD software using the bandwidth ratio matching function. However, activating this function in scans incorporating all occurring phases introduced new indexing problems especially for corundum.

The area inside the lower frame of Figure 2b is presented in a higher magnification in Figure 3 to visualize the crystallization outside the stria. The small, bright YSZ-crystals are now clearly visible. Because of the problem of separating YSZ and YAG based on their crystallography, chemistry-assisted indexing (ChI) was used to distinguish the phases in the EBSD scan performed within the area framed in the SEM-micrograph. In this process, EDX data are collected simultaneous to the EBSD patterns and later used to reindex the scan and distinguish phases based on their chemistry as well as their crystallography.[13] The achieved phase distinction enables to perform phase specific crystal orientation and texture analysis.

The presented phase+IQ map of the scan (left) shows that phase distinction was successful. It also shows that only one of

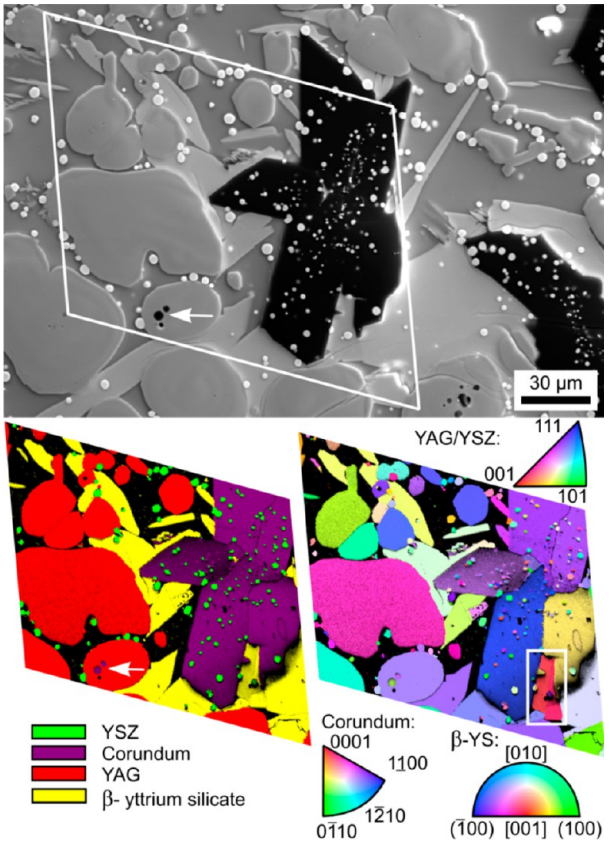

Figure 3. SEM micrograph of the microstructure in the lower frame of Figure 2b. An EBSD scan was performed inside the frame area. The phase+IQ map (left) and the IPF map (right) of the scan are presented below.

the three dark spots inside the YAG crystal (white arrow) is a pore, whereas the other two are corundum crystals with morphologies very different from that of the large corundum crystals observed throughout the sample. The correlation of the phases in this map with the orientation information presented in the IPF+IQ map presented to the right shows that the large corundum structure is in fact composed of multiple crystals of different orientations. None of the phases in this map show orientational commonalities between individual crystals. A larger area of polygon YAG was also scanned to confirm this statement with a representative number of crystals. The framed area in the IPF+IQ map contains two β-YS crystals which share a common (110) plane, i.e., twinning of this phase is observed. As this area of β-YS is almost surrounded by corundum, it seems likely that twinning occurred as a mechanism of stress relaxation either during growth or cooling.

As the YSZ crystals in Figure 3 do not show a discernible texture, it may be concluded that YSZ usually assumes the shape of small spheres. In some cases, crystallographically characteristic shapes (faceting) may be observed as shown in Figure 4. Indexing the EBSD pattern obtained from the YSZ hexagon shows that this crystal has an orientation with a (111) plane almost parallel to the cut plane of the sample as indicated by the wire frame. Hence, this crystal probably formed a cube during its growth. Note that the YSZ crystals are much smaller if embedded in corundum compared to the rest of the sample in Figures 3 and 4.

As stated before, the growth morphology of YAG is very different inside the stria. Figure 5 presents the area in the top

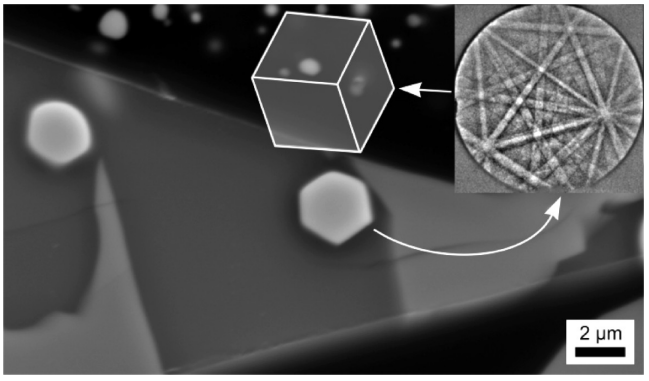

Figure 4. SEM micrograph illustrating the faceting of YSZ crystals. The EBSD pattern was obtained from the YSZ hexagon, and the wire frame of the unit cell is presented to visualize the indexed orientation.

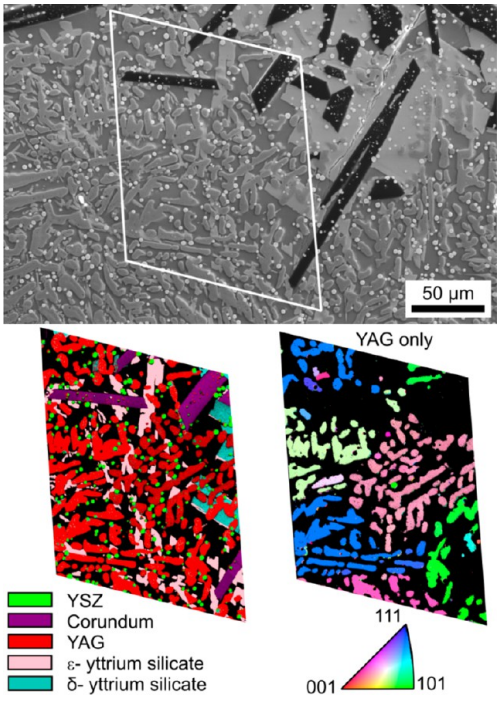

Figure 5. SEM micrograph of the microstructure in the upper frame of Figure 2b. An EBSD scan was performed inside the frame area. The phase+IQ map of the entire scan (left) is presented as well as the IPF map of YAG only (right).

frame of Figure 2b in greater detail to visualize crystal morphologies. An EBSD-scan was performed inside the framed area and reindexed using ChI to provide the phase+IQ map presented below. In addition to visualizing the achieved phase separation, this map also shows that δ-YS occurs in the core of the stria, whereas ε-YS is observed between the YAG crystals. As the morphology of YAG is of interest in this case, the selective IPF+IQ map of YAG is also presented. The observed orientation relationships and growth morphologies clearly show that the figure presents a 2D cut through 3D dendrites of YAG, i.e., a completely different growth mechanism compared to the polygon growth outside the stria. The dendritic structures in Figure 5 incorporate orientation deviations of less than 3° over distances of more than 100 μm. Similar changes in the crystal orientation were observed after the surface crystallization of YAG.[6] By comparison, much larger dendritic structures with

dx.doi.org/10.1021/am401953j | ACS Appl. Mater. Interfaces 2013, 5, 8531−8536

orientational changes of less than 5° over distances of more than 4 mm have been grown from glass melts using chemically induced nucleation.[14] Dendritic fragmentation,[15] however, was not detected in these samples.

YAG crystals showing both polygon and dendritic growth may be observed at the bulk/stria interface as shown in Figure 6. An EDX line scan (15 kV) was performed along the arrow

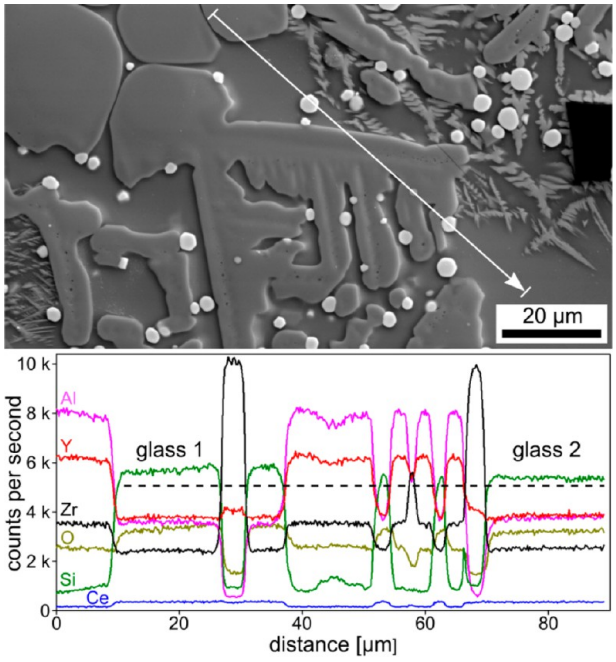

Figure 6. SEM micrograph featuring a YAG crystal showing polygon as well as dendritic growth. The results of an EDX linescan performed along the superimposed line are presented below.

and the results are presented below. Most of the indicated compositions match what would be expected of the respective crystal phase, including the low Al content in YSZ previously mentioned. However, the residual glass 1 near the polygon YAG clearly contains more Si than the residual glass 2 in the area where dendritic YAG is observed. Additionally, the residual glass and the YSZ crystals show higher Ce concentrations than YAG where it should be incorporated to cause the fluorescence expected from the material.

Figure 7 presents fluorescence micrographs of the sample exited with two different wavelength ranges: (a) 300−400 nm and (b) 450−490 nm. The strong blue fluorescence inside the stria (top) is cause by the yttrium silicates, whereas the strong yellow fluorescence results from the YAG crystals. Hence enough Ce^{3+} was incorporated into the YAG crystals to achieve the desired fluorescence. Intensity differences between dendritic and polygon YAG were not observed.

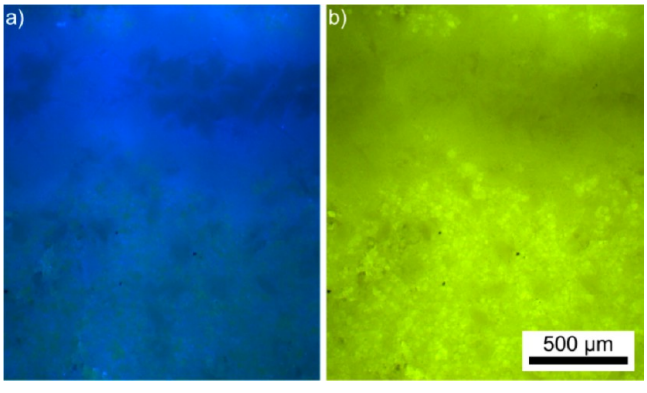

Figure 7. Fluorescence micrographs of the sample surface excited by light of the wavelengths (a) 300−400 nm and (b) 450−490 nm.

Pores are frequently observed between the crystals in the sample as seen in Figure 8, where the surface was tilted by 70°

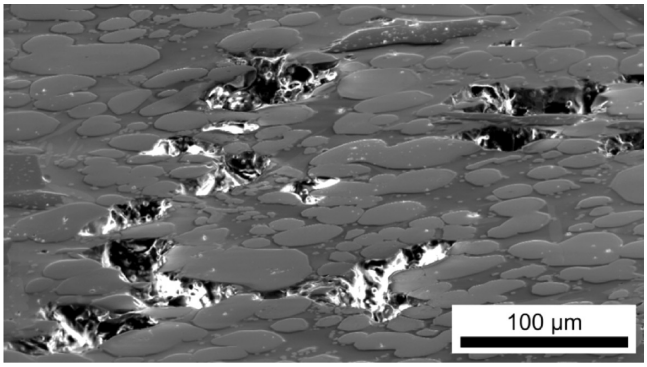

Figure 8. SEM micrograph of the sample surface tilted by 70° featuring large pores in the material.

to enhance the topographical contrast. They may be explained by the volume contraction accompanying crystal growth. Pore formation adjacent to YAG crystallization in glasses was also recently described in a surface crystallizing system.[6]

The occurrence of multiple crystalline phases in the glass-ceramics enables to optimize their properties by controlling the crystallization with respect to grain size and phase percentages.[16] The formation of YSZ and various yttrium silicates next to YAG has also been observed during the crystallization of yttrium oxynitride glasses[17] which are, however more complicated to produce as the glasses must be melted in a nitrogen atmosphere. Additionally the glass analyzed here only contains such small quantities of yttrium silicates and corundum that they fail to be detected by XRD analysis.

A clear crystallization chronology may be formulated based on the data presented above: YSZ is the first phase to crystallize as it is enclosed in all other phases. Corundum is the second phase to crystallize because the YSZ crystals inside the corundum crystals are clearly smaller than those enclosed in YAG and the residual glass, i.e., their growth was stopped earlier. The third phase to crystallize is YAG because it incorporates larger YSZ crystals. In contrast to the preferred (111)-orientation recently reported,[5] the YAG crystals presented here do not show a texture, which is in agreement to the results obtained from surface-crystallized YAG.[6] The corundum inclusions in YAG pointed out in Figure 3 show that YAG may also incorporate small corundum crystals although direct contact between YAG and corundum is otherwise rarely observed. The respective yttrium silicates nucleate on the surfaces of both corundum and YAG, i.e., they were the last phases to crystallize, possibly while the sample is cooled at the end of the annealing process.

All three YS were recently also found to crystallize in specific locations after the crystallization of YAG from a glass surface.[6] Similar to the results presented here where δ-YS formed around the corundum crystals in the stria and ε-YS appears further outside the stria, δ-YS was detected immediately next to the YAG layer where a higher number of star-shaped, Al-enriched

dx.doi.org/10.1021/am401953j | ACS Appl. Mater. Interfaces 2013, 5, 8531−8536

crystals were shown to exist[6] followed by a layer of ε-YS. The β-YS detected outside the stria was only found in the bulk of the surface crystallizing glass.[6] The crystal morphologies were very different in ref 6 because of the high number of star-shaped crystals blocking their growth.

YSZ nucleation is clearly not homogeneous in the sample, even outside the stria. Corundum crystals are always observed in an area of elevated YSZ nucleation, hence its growth is probably initiated by the local Al enrichment caused by strong local YSZ growth which does not incorporate Al, see Figure 6. YAG nucleates throughout the sample except for the core of the stria, where the density of corundum crystals is so high that the aluminum concentration in the residual glass was presumably not high enough to allow YAG crystallization.

The YAG growth mechanism in the stria differs from the crystallization outside this region. Furthermore, the EDX line scan in Figure 6 illustrates that the Si concentration is higher near the polygon YAG than near the dendritic YAG. As dendritic YAG is only observed inside the stria, it may be concluded that the SiO_2 concentration should be lower here than outside the stria. Recently, J. Du[18] reported on yttrium aluminosilicate glass with comparably low silica concentrations (5−20 mol %). It was shown that the coordination number of aluminum and yttrium decreases with increasing silica concentrations. Hence the coordination of aluminum shifts from octahedral to tetrahedral. Alumina with tetrahedral coordination enters the Si−O network and acts as network former. Aluminum in octahedral coordination would hence be preferred in the stria and then leads to a smaller local viscosity. This leads to a higher nucleation rate of YSZ, which in turn triggers the growth of corundum.

The higher Si concentration of the residual glass near the polygon YAG indicates aluminum should preferably occur in tetrahedral coordination, which would raise the local viscosity. This difference in the local viscosities could cause the observed growth mechanism change. If this is correct, it could be in agreement with the literature, where simulations showed that the growth mechanism of viscose fingering may be changed to dendritic growth by changing the viscosity of the matrix.[18,19]

The model of viscous fingering was developed for the case of two fluids with different viscosities forming interpenetrating structures. It might also be applied to explain crystal growth morphologies indicating tip splitting and possible fingering, which have been observed in glass-ceramics,[21,22] i.e., the growth mechanisms may be comparable.

It is noteworthy that YSZ is rarely surrounded by YAG but instead mostly occurs at the interface, see Figures 3−6. Hence it seems plausible that YSZ crystals are pushed along by the YAG growth front. A similar behavior has already been described in the literature where growing polymer-dendrites pushed away clay particles suspended in the aqueous polymer solution.[20] As there are much fewer YAG crystals then YSZ crystals in the described areas, it seems unlikely that YSZ acts as a nucleation agent for YAG. Nevertheless, larger nucleation rates should lead to the preferred formation of isolated YAG particles, whereas smaller nucleation rates should preferably lead to dendritic growth. The latter has its reason in a limited transport at the growth front, either in the transport of the crystallization energy from the growth front or in the diffusion of components, during which the respective crystal is formed from the growth front.

CONCLUSIONS

A glass of the composition $23.82Y_2O_3{\cdot}39.82Al_2O_3{\cdot}28.50SiO_2{\cdot}2.91AlF_3{\cdot}4.95ZrO_2$ doped with 2 mol % CeF_3 showed nucleation and subsequent crystal growth in the bulk after thermal annealing for 20 h at 1250 °C. A stria of changed chemical composition led to very different results confined to a local area. The initial and unequally distributed nucleation of YSZ leads to the crystallization of corundum where the YSZ nucleation rate is high. YAG crystals nucleate in a later stage and probably push YSZ crystals along as they grow instead of growing around them, indicating comparably slow growth. In the bulk of the glass, YAG forms polygon crystals without orientational commonalities. Inside the stria, a reduced viscosity of the glass matrix probably changes the mechanism of YAG-growth to dendritic growth. Finally, three different yttrium silicates of the composition $Y_2Si_2O_7$ nucleate preferably in the vicinity of corundum crystals. Both YAG and the yttrium silicates show fluorescence indicating the incorporation of Ce^{3+} into their structure and making this material a candidate for light transforming applications. Pores are formed because of the density increase during crystallization.

AUTHOR INFORMATION

Corresponding Author

*E-mail: wolfgang.w@uni-jena.de. Tel: (0049) 03641 948515. Fax: (0049) 03641 948502.

Notes

The authors declare no competing financial interest.

ACKNOWLEDGMENTS

The material files used for indexing the yttrium silicates were built by René de Kloe. The authors thank the Graduate Academy of the Jena University for support via the PhD scholarship "Landesgraduiertenstipendium" for this study. This work was also supported by Deutsche Forschungsgemeinschaft (DFG) in Bonn Bad Godesberg (Germany) via project nr. RU 417/14-1.

REFERENCES

(1) Fujita, S.; Tanabe, S. *Opt. Mater.* **2010**, *32*, 886−890.
(2) Keshavarzi, A.; Wisniewski, W.; Rüssel, C. *CrystEngComm.* **2012**, *14*, 6904−6909.
(3) Keshavarzi, A.; Rüssel, C. *Mater. Chem. Phys.* **2012**, *132*, 278−283.
(4) Nishiura, S.; Tanabe, S.; Fujita, S.; Fujimoto, Y. *Opt. Mater.* **2011**, *33*, 688−691.
(5) Yang, J.; Chen, B.; Pun, E. Y. B.; Zhai, B.; Lin, H. *J. Lumin.* **2013**, *134*, 622−628.
(6) Keshavarzi, A.; Wisniewski, W.; de Kloe, R.; Rüssel, C. *CrystEngComm* **2013**, *15*, 5425−5433.
(7) Nishi, M.; Tanabe, S.; Fujita, K.; Hirao, K.; Pezzotti, G. *Solid State Commun.* **2004**, *132*, 19−23.
(8) Berthier, T.; Fokin, V. M.; Zanotto, E. D. *J. Non-Cryst. Solids* **2008**, *354*, 1721−1730.
(9) Höland, W.; Beal, G. H. *Glass Ceramic Technology*; Wiley−The American Ceramic Society: Westerville, OH, 2012.
(10) de Almeida, R. P. F.; Bocker, C.; Rüssel, C. *Chem. Mater.* **2008**, *20*, 5916−5921.
(11) Bocker, C.; Bhattacharya, S.; Höche, T.; Rüssel, C. *Acta. Mater.* **2009**, *57*, 5956−5963.
(12) Hendy, S. *Appl. Phys. Lett.* **2002**, *81*, 1171−1173.
(13) Nowell, M. M.; Wright, S. I. *J. Microsc.* **2004**, *213*, 296−305.
(14) Wisniewski, W.; Nagel, M.; Völksch, G.; Rüssel, C. *Cryst. Growth Des.* **2010**, *10*, 1939−1945.

(15) Rettenmayr, M. *Int. Mater. Rev.* **2009**, *54*, 1−17.
(16) Wange, P.; Höche, T.; Rüssel, C.; Schnapp, J. D. *J. Non-Cryst. Solids* **2002**, *298*, 137−145.
(17) Vomacka, P. *J. Eur. Ceram. Soc.* **1997**, *17*, 615−621.
(18) Du, J. *J. Am. Ceram. Soc.* **2009**, *92*, 87−95.
(19) Nittmann, J.; Stanley, H. E. *Nature* **1986**, *321*, 663−668.
(20) Gránásy, L.; Pusztai, T.; Warrem, J. A.; Douglas, J. F.; Börzsönyi, T.; Ferreiro, V. *Nat. Mater.* **2003**, *2*, 92−96.
(21) Haas, S.; Hoell, A.; Wurth, R.; Rüssel, C.; Boesecke, P.; Vainio, U. *Phys. Rev. B* **2010**, *81*, 184207.
(22) Wurth, R.; Rüssel, C. *Solid State Sci.* **2011**, *13*, 1132−1136.